Optical Review (2020) 27:156–169
https://doi.org/10.1007/s10043-020-00587-8

REGULAR PAPER

OFDM tolerance to additive white Gaussian and laser phase noises in optical heterodyning systems accompanied by the feasible pilot-assisted equalization

David Zabala-Blanco[1] · Cesar A. Azurdia-Meza[2] · Samuel Montejo-Sánchez[3] · Ali Dehghan Firoozabadi[4]

Received: 6 June 2019 / Accepted: 18 February 2020 / Published online: 5 March 2020

Abstract
It is well known that the performance of orthogonal frequency division multiplexing (OFDM) is limited by phase noise, which depends on the laser linewidths for coherent-detection radio over fiber (RoF) systems. In this manuscript, we present numerical and theoretical results to analyze the combined effects of phase and additive white Gaussian noises in the performance of RoF-OFDM schemes with the feasible pilot-based channel corrector. This phase-noise compensator is adopted due to its effectiveness as well as simplicity. It is shown that as the subcarrier modulation format increases, the required radio frequency linewidth for overcoming the FEC limit decreases by a factor of 10 times. Also, there is a signal–noise ratio penalty of 7 dB. Furthermore, it is demonstrated that the bit error rate enhances as the product of the laser linewidths and OFDM symbol period decreases because the pilot-assisted equalization method acts as a high-pass filter for phase noise. We finally discovered that the intermediate-frequency (IF) carrier suppression is not mandatory; the system performance is not affected by selecting properly the carrier–signal ratio and IF. To confirm the previous observation, a novel way to measure phase noise in RoF-OFDM signals accompanied by the IF carrier is proposed. The mean integral phase noise comes from the adaptation of the root mean square phase deviation of the single-carrier systems. This work serves as a guideline for the study and design of OFDM-based RoF schemes susceptible to direct and coherent detections.

Keywords Additive white Gaussian noise · Laser phase noise · Orthogonal frequency division multiplexing · Intermediate frequency suppression · Radio over fiber systems.

1 Introduction

During the past 3 decades, the telecommunication industry has faced impressive growth not only in the number of subscribers worldwide but also in the demand for higher-speed data transmissions [1]. In fact, the bandwidth required to deliver high-speed data in the access network will grow to multi-Gigabits per second for the next years. To this end, multicarrier modulation techniques have been considered owing to their capability to convey a high-speed data stream via multiple spectral/overlapped lower-speed subcarriers [2]. In particular, power line communication (PLC), digital subscriber line (DSL), digital audio and video broadcasting (DAB/DVB), wireless fidelity (WiFi), and long term evolution (LTE) technologies, for instance, have relied for their link interfaces on orthogonal frequency division multiplexing (OFDM). OFDM is massively adopted by its robustness against multipath environments, high-spectral efficiency, and high-speed data streams [3]. Additionally, OFDM has been taken into account for new popular technologies, including the next-generation passive optical networks (NG-PON) [4], 5th generation cellular systems (5G) [1], and visible light communications (VLC) [5].

Unfortunately, OFDM implementations are prone to some disadvantages [3]. On the one hand, a very large peak–average power ratio, which drives the transmitter's

✉ David Zabala-Blanco
davidzabalablanco@hotmail.com

1 Department of Computing and Industries, Universidad Católica del Maule, 3466706 Talca, Chile

2 Department of Electrical Engineering, Universidad de Chile, 8370451 Santiago, Chile

3 Programa Institucional de Fomento a la I+D+i, Universidad Tecnológica Metropolitana, 8940577 Santiago, Chile

4 Department of Electricity, Universidad Tecnológica Metropolitana, 7800002 Santiago, Chile

power amplifier into saturation, leads to both out-of-band power and in-band distortion [6]. In this paper, we will not focus on this drawback. On the other hand, since the relatively long OFDM symbol length contrasted to that of the single-carrier signals, phase mismatch between the receiver's local oscillator and the carrier of the received signal deteriorates the bit error rate (BER) metric. The origin of phase noise is the oscillators' instabilities [7] and/or dispersion caused by the propagation channel [8]. Phase error leads to intercarrier interference (ICI), and a rotation of each subcarrier, termed common phase error (CPE). In comparison to electrical radio frequency (RF) systems, in optically up-converted OFDM signals, the involved bit rates and linewidth oscillators are much higher (in the order of Gbps and MHz, respectively). Therefore, RF analyzes cannot be extrapolated straight-forwardly to the optical domain.

OFDM-based radio over fiber (RoF) systems have been tested as the solution to support secure, cost-effective, and high-capacity vehicular/mobile /wireless access for the implementation of the next-generation wireless networks, thanks to the integration of optical fibers and millimeter-wave frequencies [10]. These schemes can be implemented via the following detection types: direct [10, 11] and coherent [12, 13]. Direct optical OFDM has a simple base station, but with the cost of a worse receiving sensitivity when contrasted with coherent optical OFDM. In direct-detection networks together with time delay pre-compensations, there is not laser linewidth penalty, since the beating fields after the photo-detection process are phase-correlated. For coherent-detection schemes, the RF linewidth is the detrimental impairment. This fact occurs as there is no phase coherence between the receiver local oscillator and carrier of the received signal. Regardless of the type of optical OFDM system, studies have concluded that the bit error rate (BER) improves as the laser linewidth and/or OFDM symbol period decrease as the phase noise variations are much slower than the duration of a single OFDM symbol [3]. Among the most famous compensators stand out the RF-pilot [14–16] and the pilot-assisted [17–19]. The former comes from the addition of an RF-pilot tone in the middle of OFDM band that is utilized at the receiver to revert ICI and CPE effects. The pilot–signal ratio as well as the spectral gap have an extreme relevance to avoid distortion resulted from the adjacent subcarriers. Meanwhile, the latter diminishes CPE by estimating the mean phase rotation of each OFDM symbol through subcarrier tones and, then, by rotating the received OFDM symbols back. The system performance improves as the number of pilot subcarriers increases. By maintaining the simplicity of the digital signal processing and effective bit rate, the pilot-assisted equalization may be useful for reducing phase noise, especially the CPE part [20, 21], see Fig. 1b. For estimating the wireless channel, pilot subcarriers are always inserted along with the data subcarriers at the transmitter (refers to the Add Pilots stage at the OFDM modulator). At the demodulator, the OFDM signal is recovered by linearly interpolating the unknown data from the demodulated pilots (the equalization process) [22]. The linear interpolation is chosen due to its simplicity and effectiveness [23]. All these processes are done OFDM symbol per OFDM symbol to track the rapid quadrature and in-phase variations in millimeter-wave RoF-OFDM networks. In [24], authors recently evaluated the impact of phase correlation between the fields at the base station on the performance of pilot-based channel correction RoF-OFDM schemes, finding three system performance behaviors in terms of the correlation degree. In these transmissions, but with/without phase coherence at the OFDM demodulator, there is a research opportunity regarding the impact of phase noise in the BER.

In this manuscript, the OFDM tolerance to the laser phase noise and the additive white Gaussian noise (AWGN) in pilot-assisted RoF-OFDM systems is theoretically and numerically evaluated. Different (1) optical up-conversion techniques [25–27], such as externally modulated laser, dual-mode lasers, and sideband injection locking, (2) configurations of the carrier–sideband ratio (CSR) and intermediate frequency (IF), and (3) subcarrier modulation formats: quadrature phase-shift keying (QPSK) and 16-ary quadrature-amplitude modulation (16QAM), are taking into account. The contributions of this work are twofold:

- By considering transmission rates in the order of Gbps, distributed feedback (DFB) lasers are suitable for QPSK, whereas external cavity lasers (ECL) must be employed for 16QAM at half the OFDM bandwidth. Between these formats, the signal–noise-ratio (SNR) cost is given by 7 dB.
- The transmitted OFDM signal can be recovered despite the IF phase noise for suitable values of the CSR and IF. Thus, the IF carrier suppression is not necessary for the optical-modulation stage. For the first time, this finding is explained via the introduction of the mean integral phase noise (MIPN), since when the IF carrier together with the OFDM signal are presented, the common phase noise measurements are useless.

Following a deductive approach, we further verify that the BER enhances as the laser linewidth narrows, bit rate increases, and/or number of subcarriers decreases. Thus, the system performance can be established in terms of the relationship between the RF linewidth and OFDM symbol period for general design purposes.

The rest of the paper is organized as follows. Section 2 presents an overall optical heterodyning system without the IF carrier suppression; performance metrics are also exposed. In Sect. 3, results are reported for numerous OFDM signals, and phase and amplitude noises. In Sect. 4,

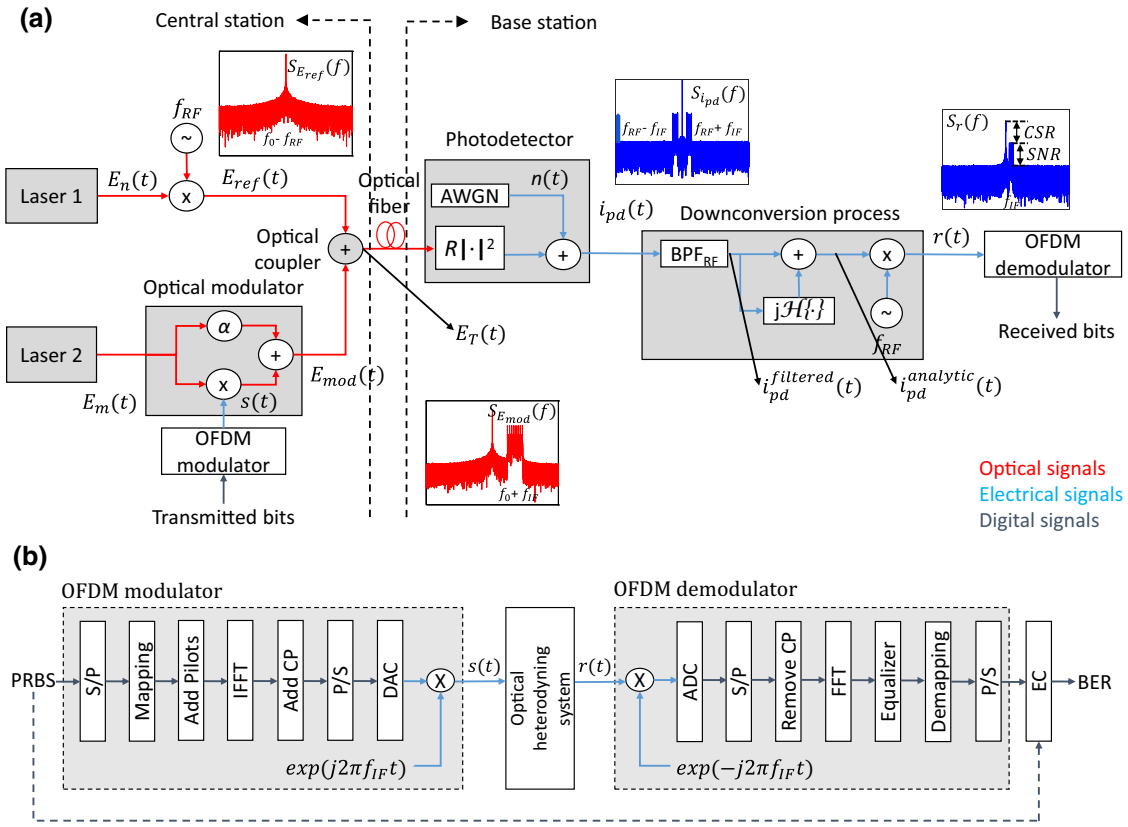

Fig. 1 **a** Block diagram of a coherent-detection RoF scheme. AWGN: additive white Gaussian noise, and $\mathrm{BPF_{RF}}$: band pass filter centered at the radio frequency. **b** OFDM modem. *PBRS* pseudo random binary sequence, *S/P* serial-to-parallel, *IFFT* inverse fast Fourier transform, *CP* cyclic prefix, *P/S* parallel-to-serial, *DAC* digital-to-analog converter, *ADC* analog-to-digital converter, *EC* error counting, and *BER* bit error rate

discussion of results is described and reported, focused on the design and implementation of RoF schemes with direct and coherent detections. Finally, conclusions are given in Sect. 5.

2 System model and methodology

2.1 Optical OFDM scheme

At the central station of an overall RoF system under coherent detection, the reference and modulated optical tones are represented as follows

$$E_{\mathrm{ref}}(t) = E_n(t)\exp(-j2\pi f_{\mathrm{RF}}t), \tag{1}$$

$$E_{\mathrm{mod}}(t) = E_m(t)[\alpha + s(t)], \tag{2}$$

where $E_i(t) = E_0\exp\{j[2\pi f_0 t + \phi_i(t)]\}$ models a laser electric field with an amplitude-stabilized E_0, an established central frequency f_0, and a phase fluctuation $\phi_i(t)$, which is a Wiener process with null mean and variance in terms of the laser linewidth parameter $\Delta\nu_i$, for $i \in \{\mathrm{mod,ref}\}$. Besides, f_{RF} denotes the RF, α allows to control the CSR at the optical-modulation stage, and $s(t) = \sum_{i=0}^{N-1} c_i \exp[j2\pi(i/T_{\mathrm{s}} + f_{\mathrm{IF}})t]$ refers to a single OFDM symbol whose duration is given by the OFDM symbol period T_{s}. The multicarrier signal comes from the sum of N subcarriers, which are modulated by symbol constellations c_i, and centered at the IF (f_{IF}). In this manuscript, we focus on the case of linear field modulation to evaluate the phase noise effects from the IF presence. Fields are then combined by a standard optical coupler, resulting total field

$$E_{\mathrm{T}}(t) = E_{\mathrm{ref}}(t) + E_{\mathrm{mod}}(t). \tag{3}$$

Afterward, this signal is conveyed through an optical fiber from the central station to the base station. The maximum transmission rate and link length mainly depend on phase error, which comes from the chromatic dispersion fiber as well as the laser source. Loss and non-linearity of the fiber also limit the relationship between the bit rate and transmission distance, but these impairments and their contributions to the system performance do not fall in this study. In this

paper, we focus on laser phase noise since there can not be additional phase error in coherent-detection RoF-OFDM networks (the reference and modulated fields are phase-uncorrelated from the base station). Namely, the chromatic dispersion can be neglected. The heterodyning signal is down-converted to the electrical domain using a photodetector subject to a square-law transfer curve, where AWGN must be inserted for accounting shot and thermal noises [3]. The electrical current results in

$$\begin{aligned} i_{\mathrm{pd}}(t) &= R|E_{\mathrm{T}}(t)|^2 + n(t) \\ &= RE_0^2\big(1 + |\alpha + s(t)|^2 + 2\Re\{\exp[2\pi f_{\mathrm{RF}}t + \phi_{\mathrm{RF}}(t)] \\ &\quad \times [\alpha + s(t)]\}\big) + n(t), \end{aligned} \tag{4}$$

with R, $n(t)$, $\phi_{\mathrm{RF}}(t) = \phi_{\mathrm{mod}}(t) - \phi_{\mathrm{ref}}(t)$, and $\Re\{\cdot\}$ being the photodetector responsivity, AWGN signal, RF phase noise, and real part function, respectively. In detail, the steps to obtain the expression (4) are exposed in the Appendix A. For perfectly correlated fields, $\Delta\nu_{\mathrm{RF}}$ matches to 0 Hz (Dirac delta functions are revealed in the spectrum). Meanwhile, for uncorrelated tones, the RF linewidth arises from the addition of the laser linewidths, i.e., $\Delta\nu_{\mathrm{RF}} = \Delta\nu_{\mathrm{mod}} + \Delta\nu_{\mathrm{ref}}$, with Lorentzian shapes in the frequency domain. For partially decorrelated fields, an extensive investigation was recently done [24]. In terms of the degree of phase-decorrelation between the tones at the transmission stage, these spectra were discovered for single carrier systems [28]. Following the down-conversion process (filtered band pass at the RF to remove the low-frequency components $i_{\mathrm{pd}}^{\mathrm{filtered}}(t)$, converted to an analytic signal $i_{\mathrm{pd}}^{\mathrm{analytic}}(t)$ by employing the Hilbert transform $\mathcal{H}\{\cdot\}$, and downconverted to the IF $r(t)$, see Fig. 1a for more information) carefully presented in Appendix A, the normalized input to the base station ($R = 1$ A/W and $E_0 = \sqrt{0.5}$ V/m [23, 24]) acquires the form of

$$r(t) = [\alpha + s(t)]\exp[j\phi_{\mathrm{RF}}(t)] + n_{\mathrm{IF}}(t), \tag{5}$$

where $n_{\mathrm{IF}}(t)$ refers to the analytic AWGN at IF. As seen, the received OFDM symbol is corrupted by phase noise as well as AWGN, which in turn introduces amplitude and phase noises. By considering the coherent approach, Fig. 1a shows the OFDM-based RoF scheme from the central station to any base station, which may represent various downlink transmission techniques [29, 30].

In regards to the simulated OFDM signal, Fig. 1b details the modulation and demodulation stages, which are based on our previous work [24]. Here, phase noise is combated via the pilot-assisted equalization method, and rectangular filters at the digital-to-analog and analog-to-digital converters are utilized to achieve optimal SNRs. For the current research, notice that the following changes are realized: (1) QPSK and 16QAM are evaluated, while higher subcarrier modulation formats are excluded owing to the adopted forward error correction (FEC) limit of 10^{-3} [31] would be unattainable according to realistic laser linewidths and OFDM symbol periods (see Sect. 3), (2) a cyclic prefix length (CP) of 1/5 is added to avoid intersymbol interference introduced by the optical and wireless channels [3], and (3) the IF is not fixed to observe and analyze the phase noise effects due to the presence of the IF carrier in the BER.

2.2 Performance metrics

Two performance metrics are used along the article to evaluate the proposed scheme. These metrics are BER and MIPN.

The system performance without the IF carrier ($\alpha = 0$) and with the matched raised cosine filters is determined by [32, 33]

$$\mathrm{BER} = \frac{2(1-\frac{1}{L})}{\log_2 L}\,\mathrm{Q}\left\{\left[\frac{6\log_2 L}{L(L^2-1)\mathrm{EVM}^2}\right]^{1/2}\right\}, \tag{6}$$

$$\mathrm{EVM} = \left[\frac{1}{\mathrm{SNR}} + 2 - 2\exp\left(-2\pi\Delta\nu_{\mathrm{RF}}T_{\mathrm{s}}\right)\right]^{1/2}, \tag{7}$$

where L represents the number of levels in each dimension of the subcarrier modulation format, $Q[\cdot]$ denotes the Gaussian co-error function [34], EVM refers to the error vector magnitude, namely the root-mean-square value of the difference between a collection of received symbols and transmitted symbols, and SNR is the signal–noise ratio. Note that the relationship between the number of data subcarriers and transmission rate establishes the duration of the OFDM symbol given the subcarrier modulation format as well as the CP [3]. Meanwhile, taking into account the pilot-based channel corrector, the system performance is determined through Monte Carlo simulation with the direct error counting method. In particular, 10^2 runs of 10^5 bits are performed for having a confidence level of 99% until BERs greater or equal than 10^{-5} [35].

On the other hand, phase noise is quantified via the introduction of a novel phase noise metric, termed as the MIPN. For single-carrier systems, a slight simplification to measure phase noise given a certain frequency offset comes from the single-sideband phase noise $\mathcal{L}(f)$, which may be seen as the noise that spreads out from the carrier as one sideband [36]. The root mean square phase deviation represents a useful approach for expressing the quality of a single broad laser [36]. It is expressed as follows

$$\Delta\phi_{\mathrm{rms}}^{SC} = \left[2\int_{f_{\mathrm{start}}}^{f_{\mathrm{stop}}} \mathcal{L}(f)\mathrm{d}f\right]^{1/2}, \tag{8}$$

where the integral limits (f_{start} and f_{stop}) define the offset-frequency region of interest according to the studied

communication technology. Instead, for OFDM signals, the phase-noise strength is calculated by the relative phase-noise bandwidth, defined as the product between the 3-dB linewidth of the local oscillator and the OFDM symbol period [37]. This measurement cannot be utilized for this investigation, where the IF carrier together with the OFDM signal is presented. Indeed, for any combination of the CSR and IF, the relative phase noise bandwidth would be the same. By adjusting over all subcarriers, the definition of the root mean square noise employed in single-carrier schemes and by discarding the impact of AWGN in the system performance, the MIPN is consequently proposed for the first time as follows

$$\begin{aligned}\Delta\phi_{\mathrm{rms}}^{\mathrm{OFDM}} &= \left[\frac{2}{N}\sum_{i=0}^{N-1}\int_{f_{\mathrm{start}}^{i}}^{f_{\mathrm{stop}}^{i}}\mathcal{L}_i(f)\mathrm{d}f\right]^{1/2}\\ &\approx\Bigg\{\frac{2}{\frac{\alpha^2\Delta\nu_{\mathrm{RF}}}{\Delta\nu_{RF}^2+[f_{\mathrm{IF}}+N/(2T_{\mathrm{s}})]^2}+\pi T_{\mathrm{s}}\coth(\pi\Delta\nu_{\mathrm{RF}}T_{\mathrm{s}})}\\ &\quad\times\left(\alpha^2\arctan\left\{\frac{\Delta\nu_{\mathrm{RF}}T_{\mathrm{s}}/2}{(\Delta\nu_{\mathrm{RF}}T_{\mathrm{s}})^2+[(f_{\mathrm{IF}}T_{\mathrm{s}}+N/2)]^2}\right\}\right.\\ &\quad\left.+\sum_{i=0}^{N-1}\arctan\left[\frac{\Delta\nu_{\mathrm{RF}}T_{\mathrm{s}}/2}{(\Delta\nu_{\mathrm{RF}}T_{\mathrm{s}})^2+(N/2-i)^2}\right]\right)\Bigg\}^{1/2},\end{aligned}\tag{9}$$

where $f_{\mathrm{start}}^{i}=f_{\mathrm{IF}}+i/T_{\mathrm{s}}$ denotes the i-th subcarrier frequency, $f_{\mathrm{stop}}^{i}=f_{\mathrm{IF}}+(i+0.5)/T_{\mathrm{s}}$ is the half of the i-th subcarrier bandwidth, and $L_i(f)=S_r(f)/S_r(f_{\mathrm{IF}}+i/T_{\mathrm{s}})$ refers to the single sideband phase noise at the i-th subcarrier. The previous boundaries are fixed for accounting the integral phase noise of each subcarrier just for once. From the expression (9), it can be seen that the new phase-noise metric depends on the CSR (α), IF (f_{IF}), number of subcarriers (N), and normalized RF linewidth ($\Delta\nu_{\mathrm{RF}}T_{\mathrm{s}}$). For an OFDM symbol, the derivation of the MIPN metric is revealed in the Appendix B.

3 Results

In this study, we evaluate the OFDM tolerance to phase noise and AWGN in optical systems with and without phase coherence between the tones at the base station. To this end, Table 1 illustrates the used parameters, which were based on [24]. In particular, we choose laser linewidths in the order of MHz and kHz to properly model DFB [38] lasers and ECLs [39], respectively. For practical purposes, the results are presented in terms of the RF carrier linewidth, which comes from the mixing process; remember that the RF linewidth is given by the arithmetic sum of each laser linewidth ($\Delta\nu_{\mathrm{RF}}=\Delta\nu_{\mathrm{mod}}+\Delta\nu_{\mathrm{ref}}$). For instance, an RF carrier with a 1-MHz linewidth might model the heterodyning of two lasers, each of a 500-kHz linewidth. For the moment, the IF carrier is suppressed ($\alpha=0$) for the sake of simplicity, and the IF is fixed to the baseband for maximizing spectral efficiency.

Table 1 Simulation parameters

Parameters	Value
Order of the laser linewidths, $\Delta\nu_{\mathrm{RF}}$	kHz, MHz
Bit rates	2.5, 5, 10 Gbps
Subcarrier modulation formats	QPSK, 16QAM
Number of data subcarriers	55, 110
Number of pilot subcarriers	9, 18
Cyclic prefix length	1/5
Oversampling factor	100 GSps

3.1 Combined effects of laser phase noise and AWGN

We present results taking into account uncorrelation and perfect-correlation cases, the latter as a BER limiting reference. For diverse bit rates and number of subcarriers, Figs. 2 and 3 reveal the BER against SNR with the RF linewidth as parameter according to different subcarrier modulation formats by QPSK and 16QAM, respectively. Whereas, solid lines consider the pilot-based channel correction method, dotted lines match to the situation of no phase-noise reduction.

Realistic results (prone to pilot-assisted equalization) are firstly explained. For a 0-Hz RF linewidth (solid curves with the circle marker), the BER does not change in terms of the OFDM parameters (transmission rate and the number of subcarriers). However, the BER depends on the number of constellation symbols, simply meaning that higher spectral efficiency formats have poorer sensitivity. In the presence of phase noise (solid curves with pentagram, square, and triangular markers), the system performance improves as the number of subcarriers decreases and/or as the bit rate increases. For instance, considering QPSK with 2-MHz linewidth and 5-Gbps transmission rate, the FEC limit cannot be reached for 128 subcarriers; whereas for 64 subcarriers, a 17-dB SNR suffices to overcome this threshold (see Fig. 2b, e). Regarding 16QAM, a 10-fold laser phase-noise reduction and an SNR penalty of 7 dB is identified with respect to QPSK. Consequently, the transmitted OFDM signal can be recovered when the SNR exceeds 24 dB. It is worth mentioning that Fig. 2b, d are identical, as well as Figs. 2c, e. Corresponding Fig. 3 also have the same behavior. Hence, the BER depends on the relationship between the bit rate and number of subcarriers, and since this ratio is inversely proportional to the OFDM symbol period (T_{s}) [3], the BER depends directly on it.

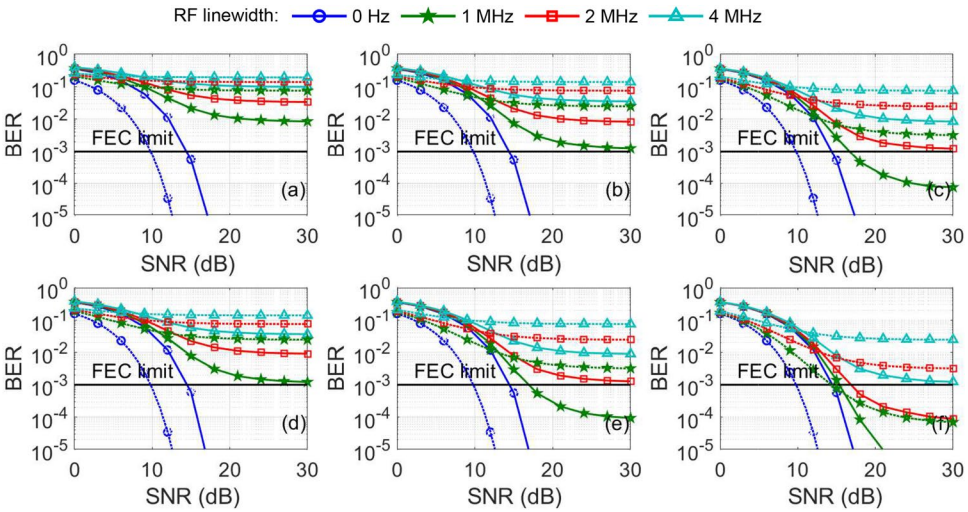

Fig. 2 BER vs. SNR with the RF linewidth as parameter for QPSK-OFDM. The bit rates and number of subcarriers correspond to **a** 2.5 Gbps and 128, **b** 5 Gbps and 128, **c** 10 Gbps and 128, **d** 2.5 Gbps and 64, **e** 5 Gbps and 64, and **f** 10 Gbps and 64, respectively. Dotted curves do not use phase-noise reduction, while solid lines utilize pilot-assisted equalization

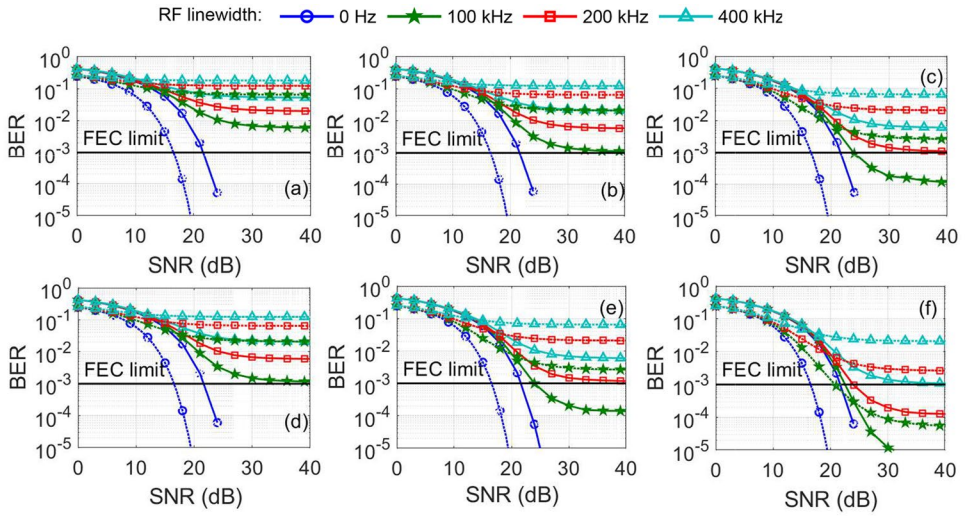

Fig. 3 BER vs. SNR with the RF linewidth as parameter for 16QAM-OFDM. The bit rates and number of subcarriers correspond to **a** 2.5 Gbps and 128, **b** 5 Gbps and 128, **c** 10 Gbps and 128, **d** 2.5 Gbps and 64, **e** 5 Gbps and 64, and **f** 10 Gbps and 64, respectively. Dotted curves do not use phase-noise reduction, while solid lines utilize pilot-assisted equalization

Comparing the dotted curves (without phase-error reduction) with the solid lines (with pilot-assisted equalization), it may be seen the BER improvement resulted from the phase-noise compensator. The pilot-based channel correction effect is superior as the product between the RF linewidth and OFDM symbol period ($\Delta\nu_{\mathrm{RF}}T_{\mathrm{s}}$) increases, because of CPE dominating over ICI [17]. For a null laser linewidth, the previous BER behavior does not happen as the theoretical and experimental BERs have different pulse shaping filters to combat AWGN, see Sect. 2. As noted for solid curves, dotted lines confirm that (1) the system performance improves as the OFDM symbol period decreases, and (2) between 16QAM and QPSK formats, the SNR penalty corresponds to 7 dB as long as 10 times the linewidth is diminished.

3.2 Pilot-assisted phase estimation

The previous result, namely the degradation system falls as the bit rate per number of subcarriers decreases, can be explained to a worse phase tracking resulted from the pilot-based equalization for longer OFDM symbol periods. Figure 4a, b represent the simulated and estimated phases for some OFDM symbol periods considering high and low AWGN values. For demonstration purposes, QPSK scheme with an RF linewidth of 2 MHz is adopted. During a single OFDM symbol, the phase-noise compensator can be modeled by subtracting the phase mean value to the phase error fluctuations (CPE mitigation). Consequently, the residual phase errors (ICI + CPE not mitigated) accompanied by its standard deviation σ,

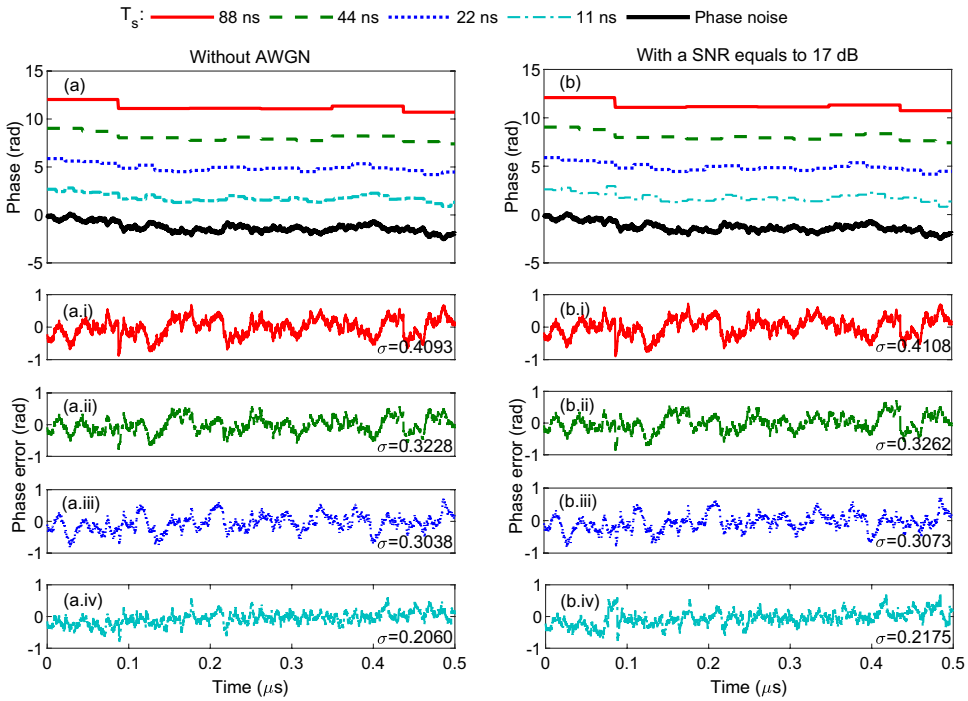

Fig. 4 With the OFDM symbol period as parameter, simulated and estimated phases **a** in the absence of AWGN and **b** in the presence of 17-dB SNR. A relative π offset is added between curves for enabling visibility. Subfigures: phase error accompanied by its standard deviation for each of the studied OFDM symbol periods. For all these observations, the QPSK scheme with a 2-MHz RF linewidth is considered

are displayed in Fig. 4i–iv. We distinguished that both measurements decrease (the BER improves) as the OFDM symbol period decreases (the number of subcarriers decreases or bit rate augments). The reason behind these outcomes come from that as the OFDM symbol period decreases, the low-frequency components of phase noise (mainly CPE) disappear, thanks to the pilot-based channel correction technique. In the presence of AWGN, the remaining phase fluctuations increase because of AWGN also contributes to CPE as well as ICI, see Eq. (5). For this observation, an SNR of 17 dB is adopted for demonstration purposes.

3.3 RF linewidth and SNR requirements for reaching the BER threshold

The RF linewidth and SNR requirements at the FEC limit with the OFDM symbol period as parameter are shown in Fig. 5. For the same OFDM symbol period, results for —16QAM and QPSK modulations are obviously different owing to constellation symbols of 16QAM are closer than QPSK. The minimum SNRs, respectively, correspond to 15 dB and 22 dB for QPSK and 16QAM. Below these values, the system performance is limited by AWGN. As the SNR increases, the use of noisier lasers also augments. Above 25-dB SNR for QPSK and 32-dB SNR for 16QAM, the BER threshold remains unattainable by the laser phase

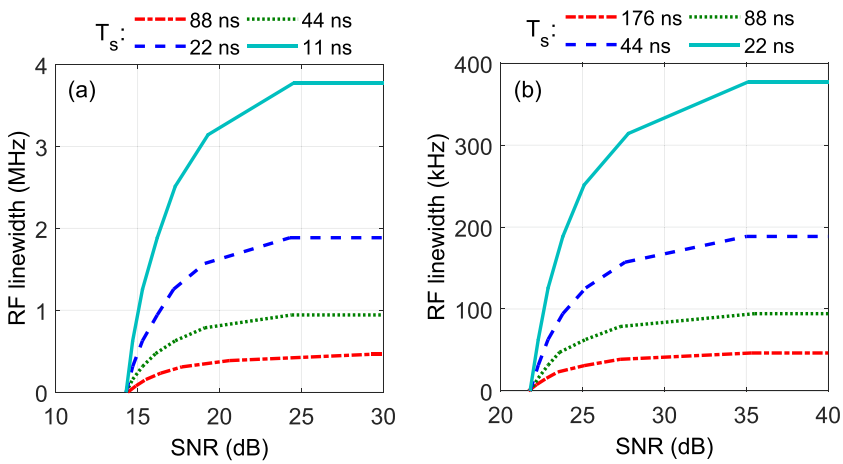

Fig. 5 The RF linewidth and SNR requirements for a BER $= 10^{-3}$ with the OFDM symbol period as parameter according to the following subcarrier modulation formats: **a** QPSK and **b** 16QAM

noise. According to the smallest OFDM symbol periods, the maximum RF linewidths are 3.8 MHz for QPSK and 380 kHz for 16QAM. If the duration of a single OFDM symbol is halved, the RF linewidth requirement is relaxed by a factor of two. As a consequence, the system performance depends on the relationship between the RF linewidth and OFDM symbol period ($\Delta\nu_{RF}T_s$).

3.4 Impact of the noise source on the system performance

The AWGN and laser phase noise effects in the reception of OFDM signal with the product of the RF linewidth and the OFDM symbol period ($\Delta\nu_{RF}T_s$) as parameter are depicted in Fig. 6. For achieving a fair comparison between the noises, the noise power spectral density is set to − 153 dB/Hz for QPSK and − 157 dB/Hz for 16QAM. The OFDM power is fixed to − 7 dBm. Therefore, the SNR is inversely proportional to the signal bandwidth and directly proportional to the symbol period. It is the reason because the BER increases as the normalized linewidth decreases for only AWGN case (dotted curves). The FEC limit is achieved as long as $\Delta\nu_{RF}T_s$ exceeds 11×10^{-3} (SNRs greater than 15 dB) for QPSK, and 2.2×10^{-3} (SNRs greater than 22 dB) for 16QAM. Meanwhile, in the presence of amplitude and phase errors (dashed curves), the superior $\Delta\nu_{RF}T_s$ matches to 22×10^{-3} (SNR = 18 dB) for QPSK, and 4.4×10^{-3} (SNR = 25 dB) for 16QAM. Finally, for only laser phase noise situation (solid curves), the BER threshold may be surpassed subject to $\Delta\nu_{RF}T_s < 44\times10^{-3}$ for QPSK and $\Delta\nu_{RF}T_s < 8.8\times10^{-3}$ for 16QAM. Here, the SNR axis is meaningless. At the same time, in Fig. 6, the identified points denote the BER at the best OFDM symbol period with amplitude and phase noises for the diverse noise types. This BER values are illustrated via constellations in Fig. 6. Constellations with both noises possess more dispersion and, as expected, the BER is worse. In contrast, constellations with only AWGN are more disperse than constellations with only laser phase noise, but this assumption is not valid as these noises have different probability distribution functions [40].

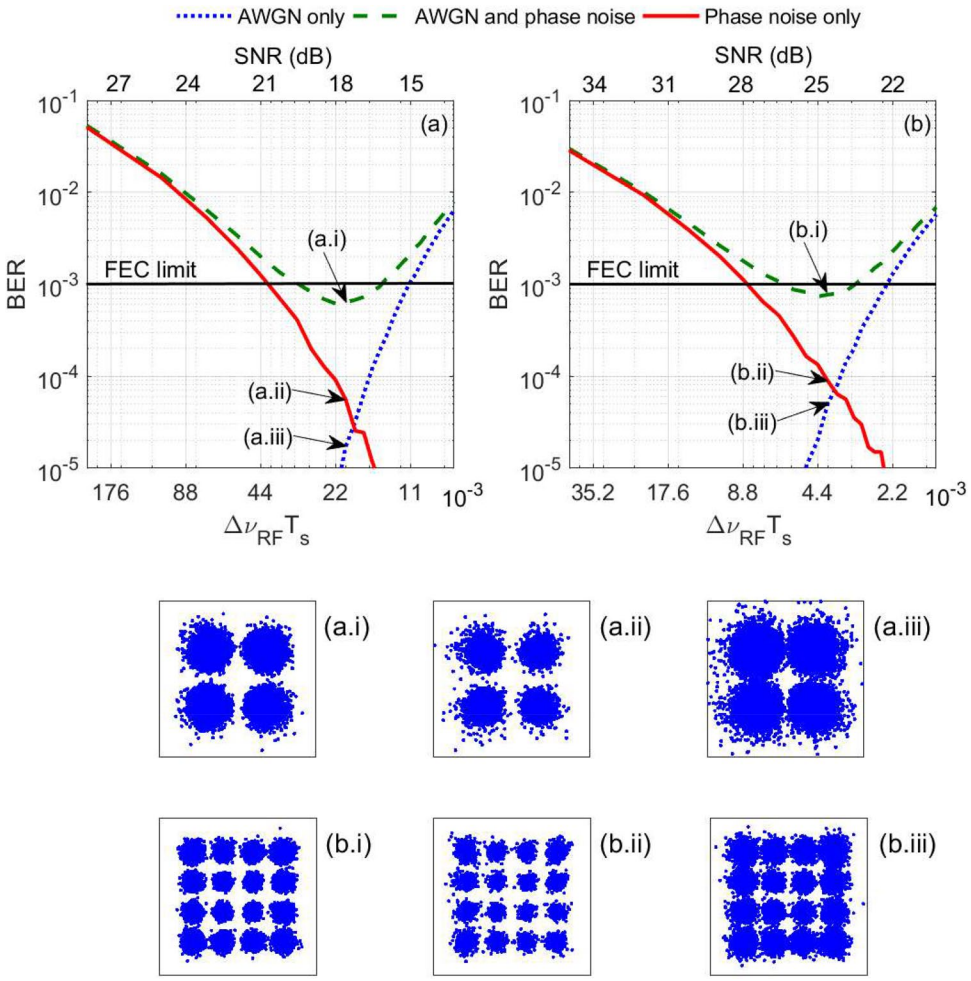

Fig. 6 BER as a function of the the normalized RF linewidth and SNR for distinct noise sources. By considering a -7 dBm OFDM signal power, the subcarrier modulation format and noise power spectral density are **a** QPSK and -153 dB/Hz, and **b** 16QAM and -157 dB/Hz, respectively. Constellations **a.i**–**a.iii** and **b.i**–**b.iii** correspond to QPSK and 16QAM schemes, respectively

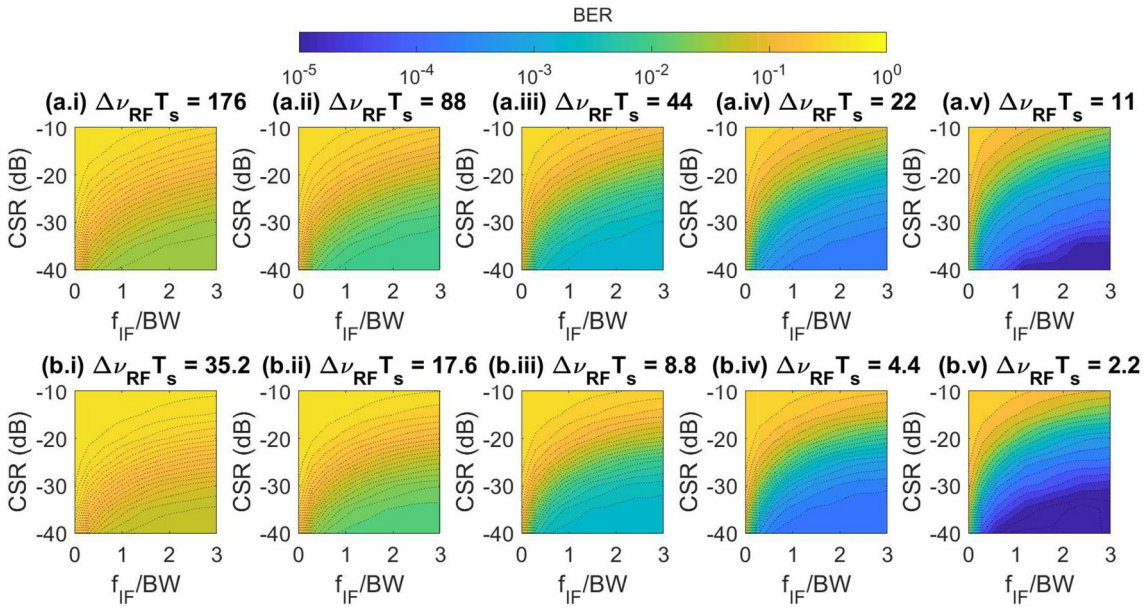

Fig. 7 For various normalized RF linewidths expressed in the order of 10^{-3}, the BER is a function of the CSR and the ratio of the IF and signal bandwidth taking into account **a** QPSK-OFDM and **b** 16QAM-OFDM schemes. The analysis does not include AWGN deterioration

3.5 Phase noise induced by the IF carrier

For many normalized RF linewidths expressed in the order of 10^{-3}, Fig. 7 depicts the BER in terms of the CSR and normalized IF [the IF divided by the signal bandwidth (BW)] for (a) QPSK and (b) 16QAM schemes. To focus on phase noise owing to the IF carrier and its impact on the BER metric, AWGN is discarded. The BER improves as the CSR and/or IF increase. It occurs as the IF moves further away from the OFDM signal, the in-band contribution of its phase noise decreases. We also learn that the IF carrier suppression is unnecessary for no BER degradation, as long as the CSR and IF parameters are properly established. For example, the system performance is not affected by phase noise which resulted from the IF carrier when the CSR is less than − 35 dB and the normalized IF is greater than 2.5. This result is explained through the novel phase-noise metric introduced in Sect. 2.2. Taking into account (a) QPSK and (b) 16QAM formats, the MIPN as a function of the CSR and IF with the normalized RF linewidth as parameter is displayed in Fig. 8. This metric proves that for the OFDM performance, the IF carrier effect can be negligible for some values of the CSR and IF. Notice that the observations regarding the simulated BER and theoretical MIPN are not exactly the same by the presence and absence of the pilot-assisted equalization, CP, and pulse shaping filters, respectively. Furthermore, it is demonstrated that the system performance critically depends on the normalized RF linewidth and subcarrier modulation format, as could be noted by theoretical curves in Figs. 2 and 3. Finally, it is confirmed that the system performance enhances for narrow laser linewidths and for few symbol constellations.

4 Discussion of results

According to the proposed system model, our results can be useful for the study and design of numerous RoF systems [29, 30] with low complexity and high precision, i.e., by employing pilot-based channel corrector.

In the downlink transmission technique by mixing two uncorrelated lasers, optical tones at the transmitter are already completely phase-decorrelated and, therefore, phase noise resulted from the fiber chromatic dispersion results negligible [25, 26]. This method is laser linewidth sensitive; recall from Sects. 3.1, 3.2, and 3.4, a decrease of 10 times of the RF linewidth enables to double the spectral efficiency prone to an SNR penalty of 7 dB. Considering practical bit rates and number of subcarriers in optical communication networks, DFB lasers can be used with QPSK-OFDM. To match the performance in 16QAM-OFDM, ECLs are the right ones. For a point-to-point link, the FEC threshold is achieved by normalized RF linewidths less than 44×10^{-3} for QPSK and 8.8×10^{-3} for 16QAM, refer to solid lines in Fig. 6. However, the laser linewidth tolerance could be relaxed by employing the well-known RF-pilot-based phase-noise compensation method [14–16], where a DC tone is inserted leaving an RF guard band between it and the OFDM signal. For this purpose, the IF carrier presence could be an attractive solution in terms of bandwidth-consuming pilot tones, but its study is left for

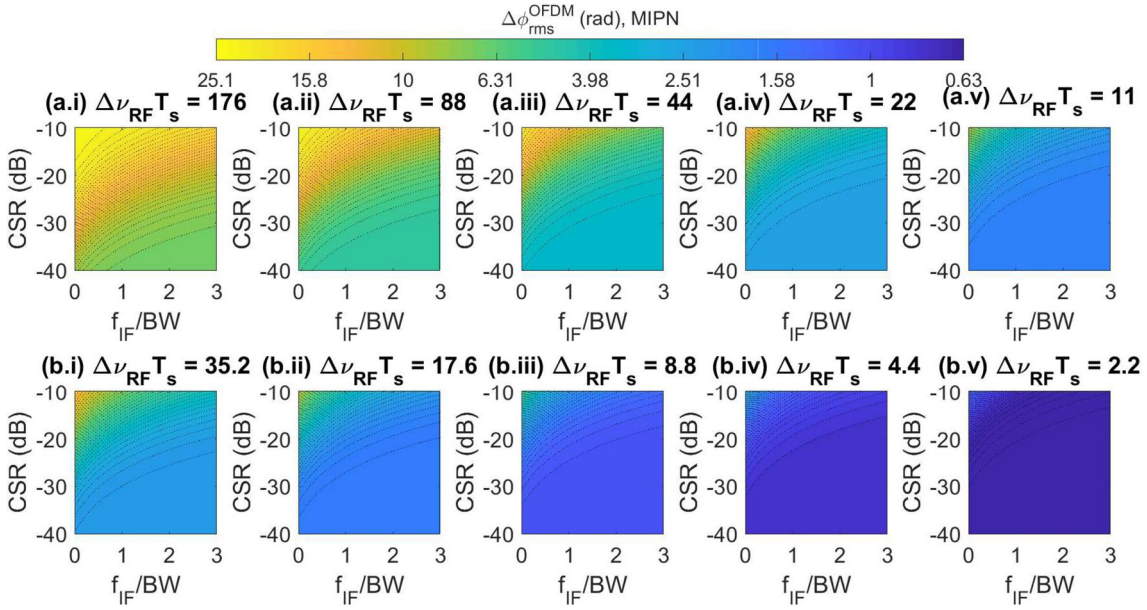

Fig. 8 With the normalized RF linewidth expressed in the order of 10^{-3} as parameter, the MIPN is in terms of the CSR and normalized IF for the following subcarrier modulation formats: **a** QPSK and **b** 16QAM. In the propagation channel, the SNR tends to infinity

future work. For now, Sect. 3.5 reveals for the first time that by setting the CSR and IF, the system performance does not experiment deterioration by the IF phase noise. Evidently, the lowest values of both parameters are the most convenient from the point of view of power and spectral efficiencies. Due to the standard phase noise measurement for OFDM systems do not consider the presence of the OFDM signal accompanied by the IF carrier, the no BER deterioration by the IF phase noise is confirmed by the MIPN, which comes from the root mean square phase error for single-carrier systems. As another pending task, based on this novel phase noise metric, the theoretical BER performance could be determined.

In [27], the sideband injection locking is investigated as a generation method based on optical up-conversion, where two slave lasers become phase-correlated through the controlled injection from a modulated master laser. The system performance of such technique is laser linewidth insensitive because as long as the slave lasers remain stably locked to the modulation sidebands of the master laser, they share phase coherence. At this scenario, the BER behavior is shown in Figs. 2, 3, 5 and 6 with null linewidths. From Fig. 5, we determine the SNR requirement at the FEC limit: 15 dB for QPSK and 22 dB for 16QAM. These performances do not depend on the OFDM symbol period. Nevertheless, when the signal power and noise power spectral density can not be controlled, the BER deteriorates as the product between the RF linewidth and OFDM symbol period increases, see dotted curves of Fig. 6. Above $\Delta\nu_{RF}T_s = 11 \times 10^{-3}$ and $\Delta\nu_{RF}T_s = 2.2 \times 10^{-3}$ for QPSK and 16QAM, respectively, there can be a successful communication.

5 Conclusions

In this manuscript, we observed and evaluated the coherent-detection RoF-OFDM signals corrupted by the laser phase noise and AWGN, and assisted by the feasible pilot-based equalization method. Numerical results depicted that in the presence of the laser phase noise, the BER improves as the number of subcarriers decreases and bit rate increases, namely for small OFDM symbol periods. Meanwhile, the BER does not depend on the OFDM symbol period given a laser linewidth of 0 Hz. These facts are because the pilot-assisted channel corrector acts as a high-pass filter for phase noise during a single OFDM symbol. Also, we learned that for standard transmission rates in the order of Gbps, there is an SNR penalty of 7 dB between QPSK and 16QAM subcarrier modulation formats to overcome the FEC limit. For QPSK-OFDM schemes, DFB lasers are suitable. Meanwhile, 16QAM-OFDM systems demand the use of ECLs. In the case of not being able to control the power of the RoF-OFDM signal (non-common context), the BER is minimized under a certain relationship between the RF linewidth and OFDM symbol period as long as phase and amplitude noises are presented. Otherwise, the BER enhances as the normalized RF linewidth augments for the case of only AWGN. It is worth indicating that performance evaluations can be presented in terms of this metric to facilitate the design and implementation stages. Finally, theoretical and simulated results show that phase noise induced by the IF carrier can be negligible by controlling CSR and IF values. For this observation, the MIPN should be introduced, since no

phase-noise metrics exist for OFDM signals in combination with the IF carrier. Finally, we believe that this manuscript will have an impact in the analysis and evaluation of RoF-OFDM schemes because perfect phase correlation in the optical fields at the central station along with pilot-assisted equalization is normally present.

Acknowledgements This work was partially supported by Laboratory of Technological Research in Pattern Recognition (LITRP), Project FONDECYT Iniciacion No. 11160517, FONDECYT Postdoctorado No. 3170021, and FONDECYT Postdoctorado No. 3190147.

Appendix 1

After the photo-detection process, the electrical current is given by

$$i_{\mathrm{pd}}(t) = R|E_{\mathrm{T}}(t)|^2 + n(t). \tag{10}$$

By inserting the total field in Eq. (10), it may be written as

$$i_{\mathrm{pd}}(t) = R|E_{\mathrm{ref}}(t) + E_{\mathrm{mod}}(t)|^2 + n(t). \tag{11}$$

By using the well-known relationships in the complex domain ($|z|^2 = zz^*$, $(z_1 + z_2)^* = z_1^* + z_2^*$, and $\Re(z) = \frac{z+z^*}{2}$, where z, z_1, and z_2 represent overall complex numbers, and $*$ denotes the conjugate operator) and taking into account that $E_{\mathrm{ref}}(t)$ and $E_{\mathrm{mod}}(t)$ correspond to complex signals, the photo-generated current acquires the form of

$$\begin{aligned} i_{\mathrm{pd}}(t) &= R[E_{\mathrm{ref}}(t) + E_{\mathrm{mod}}(t)][E_{\mathrm{ref}}(t) + E_{\mathrm{mod}}(t)]^* + n(t) \\ &= R[E_{\mathrm{ref}}(t) + E_{\mathrm{mod}}(t)][E_{\mathrm{ref}}(t)^* + E_{\mathrm{mod}}(t)^*] + n(t) \\ &= R[E_{\mathrm{ref}}(t)E_{ref}(t)^* + E_{\mathrm{ref}}(t)E_{\mathrm{mod}}(t)^* + E_{\mathrm{mod}}(t)E_{\mathrm{ref}}(t)^* \\ &\quad + E_{\mathrm{mod}}(t)E_{\mathrm{mod}}(t)^*] + n(t) \\ &= R[|E_{\mathrm{ref}}(t)|^2 + 2\Re\{E_{\mathrm{ref}}(t)^*E_{\mathrm{mod}}(t)\} + |E_{\mathrm{mod}}(t)|^2] + n(t). \end{aligned} \tag{12}$$

By considering the expressions of the reference and modulated optical tones, it can be expressed as follows

$$\begin{aligned} i_{\mathrm{pd}}(t) = R(E_0^2 + 2\Re\{E_0^2 \exp\{j[2\pi f_{\mathrm{RF}}t + \phi_{\mathrm{mod}}(t) - \phi_{\mathrm{ref}}(t)]\}[\alpha + s(t)]\} \\ + E_0^2|\alpha + s(t)|^2) + n(t). \end{aligned} \tag{13}$$

Through a band pass filter centered at RF, the low frequencies are then discarded in Eq. (13), namely

$$i_{\mathrm{pd}}^{\mathrm{filtered}}(t) = 2RE_0^2\Re\{\exp\{j[2\pi f_{\mathrm{RF}}t + \phi_{\mathrm{RF}}(t)]\}[\alpha + s(t)]\} + n_{\mathrm{RF}}(t), \tag{14}$$

where $\phi_{\mathrm{RF}}(t) = \phi_{\mathrm{mod}}(t) - \phi_{\mathrm{ref}}(t)$ refers to the RF phase noise and $n_{\mathrm{RF}}(t)$ represents the filtered AWGN. Keeping in mind the definition of the transmitted OFDM symbol (see Sect. 2.1) as well as the Euler's formula for any real number t ($\exp(jt) = \cos(t) + j\sin(t)$), the previous signal results in

$$\begin{aligned} i_{\mathrm{pd}}^{\mathrm{filtered}}(t) &= 2RE_0^2\Re\{\exp\{j[2\pi f_{\mathrm{RF}}t + \phi_{\mathrm{RF}}(t)]\} \\ &\quad \times \left\{\alpha + \sum_{i=0}^{N-1} c_i \exp[j2\pi(i/T_{\mathrm{s}} + f_{\mathrm{IF}})t]\}\right\} + n_{\mathrm{RF}}(t) \\ &= 2RE_0^2\Re\{\alpha \exp\{j[2\pi f_{\mathrm{RF}}t + \phi_{\mathrm{RF}}(t)]\} \\ &\quad + \sum_{i=0}^{N-1} c_i \exp\{j[2\pi(i/T_{\mathrm{s}} + f_{\mathrm{IF}} + f_{\mathrm{RF}})t + \phi_{\mathrm{RF}}(t)]\}\right\} + n_{\mathrm{RF}}(t) \\ &= 2RE_0^2\{\alpha \cos[2\pi f_{\mathrm{RF}}t + \phi_{\mathrm{RF}}(t)] \\ &\quad + \sum_{i=0}^{N-1} c_i \cos[2\pi(i/T_{\mathrm{s}} + f_{\mathrm{IF}} + f_{\mathrm{RF}})t + \phi_{\mathrm{RF}}(t)]\right\} + n_{\mathrm{RF}}(t). \end{aligned} \tag{15}$$

In order to recover the quadrature component of OFDM symbols, the analytical representation of the filtered photocurrent must be obtained, which is given by

$$i_{\mathrm{pd}}^{analytic}(t) = i_{\mathrm{pd}}^{\mathrm{filtered}}(t) + j\mathcal{H}\{i_{\mathrm{pd}}^{\mathrm{filtered}}(t)\}, \tag{16}$$

with $\mathcal{H}\{\cdot\}$ being the Hilbert transform. Based on the useful transformation $\mathcal{H}\{\cos(t)\} = \sin(t)$ [34], the analytic signal acquires the form of

$$\begin{aligned} i_{\mathrm{pd}}^{analytic}(t) &= 2RE_0^2\left\{\alpha \cos[2\pi f_{\mathrm{RF}}t + \phi_{\mathrm{RF}}(t)] \right. \\ &\quad \left. + \sum_{i=0}^{N-1} c_i \cos[2\pi(i/T_{\mathrm{s}} + f_{\mathrm{IF}} + f_{\mathrm{RF}})t + \phi_{\mathrm{RF}}(t)]\right\} + n_{\mathrm{RF}}(t) \\ &\quad + j2RE_0^2\{\alpha \sin[2\pi f_{\mathrm{RF}}t + \phi_{\mathrm{RF}}(t)] \\ &\quad + \sum_{i=0}^{N-1} c_i \sin[2\pi(i/T_{\mathrm{s}} + f_{\mathrm{IF}} + f_{\mathrm{RF}})t + \phi_{\mathrm{RF}}(t)]\} + j\mathcal{H}\{n_{\mathrm{RF}}(t)\} \\ &= 2RE_0^2\left(\alpha\{\cos[2\pi f_{\mathrm{RF}}t + \phi_{\mathrm{RF}}(t)] + j\sin[2\pi f_{\mathrm{RF}}t + \phi_{\mathrm{RF}}(t)]\}\right. \\ &\quad + \sum_{i=0}^{N-1} c_i \cos[2\pi(i/T_{\mathrm{s}} + f_{\mathrm{IF}} + f_{\mathrm{RF}})t + \phi_{\mathrm{RF}}(t)] \\ &\quad \left. + j\sum_{i=0}^{N-1} c_i \sin[2\pi(i/T_{\mathrm{s}} + f_{\mathrm{IF}} + f_{\mathrm{RF}})t + \phi_{\mathrm{RF}}(t)]\right) \\ &\quad + n_{\mathrm{RF}}(t) + j\mathcal{H}\{n_{\mathrm{RF}}(t)\} \\ &= 2RE_0^2\left(\alpha \exp\{j[2\pi f_{\mathrm{RF}}t + \phi_{\mathrm{RF}}(t)]\}\right. \\ &\quad \left. + \sum_{i=0}^{N-1} c_i \exp\{j[2\pi(i/T_{\mathrm{s}} + f_{\mathrm{IF}} + f_{\mathrm{RF}})t + \phi_{\mathrm{RF}}(t)]\}\right) \\ &\quad + n_{\mathrm{RF}}^{\mathrm{analytic}}(t), \end{aligned} \tag{17}$$

where $n_{\mathrm{RF}}^{\mathrm{analytical}}(t) = n_{\mathrm{RF}}(t) + j\mathcal{H}\{n_{\mathrm{RF}}(t)\}$ denotes the analytical representation of $n_{\mathrm{RF}}(t)$.

Finally, the input to the OFDM demodulator after the down-conversion process at the IF can be obtained as follows

$$
\begin{aligned}
r(t) &= i_{\mathrm{pd}}^{\mathrm{analytical}}(t)\exp(-j2\pi f_{\mathrm{RF}}t)\\
&= 2RE_0^2\left(\alpha\exp[j\phi_{\mathrm{RF}}(t)] + \sum_{i=0}^{N-1} c_i \exp\{j[2\pi(i/T_{\mathrm{s}} + f_{\mathrm{IF}})t + \phi_{\mathrm{RF}}(t)]\}\right)\\
&\quad + n_{\mathrm{RF}}^{\mathrm{analytical}}(t)\exp(-j2\pi f_{\mathrm{RF}}t)\\
&= 2RE_0^2\left(\alpha + \sum_{i=0}^{N-1} c_i \exp\{j[2\pi(i/T_{\mathrm{s}} + f_{\mathrm{IF}})t + \phi_{\mathrm{RF}}(t)]\}\right)\exp[j\phi_{\mathrm{RF}}(t)]\\
&\quad + n_{\mathrm{RF}}^{\mathrm{analytical}}(t)\exp(-j2\pi f_{\mathrm{RF}}t)\\
&= 2RE_0^2[\alpha + s(t)]\exp[j\phi_{\mathrm{RF}}(t)] + n_{\mathrm{IF}}(t),
\end{aligned}
\tag{18}
$$

with $n_{\mathrm{IF}}(t)$ being the analytic AWGN at IF.

Appendix 2

In order to focus on the RF carrier and its contribution in the BER metric, AWGN is discarded. Hence, the electrical OFDM signal at the base station acquires the form of

$$
r(t) = \left\{\alpha + \sum_{i=0}^{N-1} c_i \exp[j2\pi(i/T_{\mathrm{s}} + f_{\mathrm{IF}})t]\right\}\exp[j\phi_{\mathrm{RF}}(t)]. \tag{19}
$$

By applying the Wiener–Khinchine theorem [34], assuming that all data symbols are uncorrelated [41], and considering the Lorentzian frequency profile of the laser source [28], its power spectral density results in

$$
\begin{aligned}
S_r(f) &= \mathcal{F}\{< r^*(t)r(t+\tau) >\}\\
&= \frac{\alpha^2\Delta\nu_{\mathrm{RF}}}{\pi(\Delta\nu_{RF}^2 + f^2)} + \sum_{i=0}^{N-1}\frac{\Delta\nu_{\mathrm{RF}}}{\pi[\Delta\nu_{\mathrm{RF}}^2 + (f - i/T_{\mathrm{s}} - f_{\mathrm{IF}})^2]}.
\end{aligned}
\tag{20}
$$

By adopting the root mean square phase error from single carrier signals to OFDM systems, the MIPN may be written as

$$
\begin{aligned}
\Delta\phi_{rms}^{OFDM} &= \left[\frac{2}{N}\sum_{i=0}^{N-1}\int_{f_{\mathrm{IF}}+i/T_{\mathrm{s}}}^{f_{\mathrm{IF}}+(i+0.5)/T_{\mathrm{s}}}\frac{S_r(f)}{S_r(f_{\mathrm{IF}}+i/T_{\mathrm{s}})}df\right]^{1/2}\\
&= \left[\frac{2}{N}\sum_{i=0}^{N-1}\left(\left\{\alpha^2\arctan\left[\frac{\Delta\nu_{\mathrm{RF}}T_{\mathrm{s}}/2}{(\Delta\nu_{\mathrm{RF}}T_{\mathrm{s}})^2 + (f_{\mathrm{IF}}T_{\mathrm{s}} + i + 1/2)(f_{\mathrm{IF}}T_{\mathrm{s}} + i)}\right]\right.\right.\\
&\quad \left.\left. + \sum_{j=0}^{N-1}\arctan\left[\frac{\Delta\nu_{\mathrm{RF}}T_{\mathrm{s}}/2}{(\Delta\nu_{\mathrm{RF}}T_{\mathrm{s}})^2 + (i-j+1/2)(i-j)}\right]\right\}\right.\\
&\quad \left.\times\left\{\frac{\alpha^2\Delta\nu_{\mathrm{RF}}}{\Delta\nu_{RF}^2 + (f_{\mathrm{IF}} + i/T_{\mathrm{s}})^2} + \sum_{j=0}^{N-1}\frac{\Delta\nu_{\mathrm{RF}}}{\Delta\nu_{\mathrm{RF}}^2 + [(i-j)/T_{\mathrm{s}}]^2}\right\}^{-1}\right)\right]^{1/2}\\
&\approx \left\{\frac{2}{\frac{\alpha^2\Delta\nu_{\mathrm{RF}}}{\Delta\nu_{RF}^2 + [f_{\mathrm{IF}} + N/(2T_{\mathrm{s}})]^2} + \pi T_{\mathrm{s}}\coth(\pi\Delta\nu_{\mathrm{RF}}T_{\mathrm{s}})}\right.\\
&\quad \times\left(\alpha^2\arctan\left\{\frac{\Delta\nu_{\mathrm{RF}}T_{\mathrm{s}}/2}{(\Delta\nu_{\mathrm{RF}}T_{\mathrm{s}})^2 + [(f_{\mathrm{IF}}T_{\mathrm{s}} + N/2)]^2}\right\}\right.\\
&\quad \left.\left.+ \sum_{i=0}^{N-1}\arctan\left[\frac{\Delta\nu_{\mathrm{RF}}T_{\mathrm{s}}/2}{(\Delta\nu_{\mathrm{RF}}T_{\mathrm{s}})^2 + (N/2-i)^2}\right]\right)\right\}^{1/2}.
\end{aligned}
\tag{21}
$$

The previous approximation comes from the next assumptions: (1) the central subcarrier behavior can approximate the integral OFDM performance, and (2) the OFDM signal has several subcarriers.

References

1. Guan, P., Wu, D., Tian, T., Zhou, J., Zhang, X., Gu, L., Benjebbour, A., Iwabuchi, M., Kishiyama, Y.: 5G field trials: OFDM-based waveforms and mixed numerologies. IEEE J. Sel. Areas Commun. **35**(6), 1234–1243 (2017)
2. Tao, Y., Liu, L., Liu, S., Zhang, Z.: A survey: several technologies of non-orthogonal transmission for 5G. China Commun. **12**(10), 1–15 (2015)
3. Djordjevic, I.B.: Advanced Optical and Wireless Communications Systems. Springer, Cham (2018)
4. Obite, F., Jaja, E.T., Ijeomah, G., Jahun, K.I.: The evolution of ethernet passive optical network (EPON) and future trends. Optik **167**, 103–120 (2018)
5. Dehghan Firoozabadi, A., Azurdia-Meza, C., Soto, I., Seguel, F., Krommenacker, N., Iturralde, D., Charpentier, P., Zabala-Blanco, D.: A novel frequency domain visible light communication (VLC) three-dimensional trilateration system for localization in underground mining. Appl. Sci. **9**, 7 (2019)
6. Wang, D., Zou, N., Cui, G., Yang, Y., Namihira, Y., Zhang, Y.: Companding scheme for peak-to-average power ratio reduction in optical orthogonal frequency division multiplexing systems. Opt. Rev. **19**(6), 371–375 (2012)
7. Elwan, H.H., Khayatzadeh, R., Shao, T., Poette, J., Cabon, B., Barry, L.P.: Impact of laser mode partition noise on optical heterodyning at millimeter-wave frequencies. J. Lightw. Technol. **34**(18), 4278–4284 (2016)
8. Shao, T., Martin, E., Anandarajah, P.M., Browning, C., Vujicic, V., Llorente, R., Barry, L.P.: Chromatic dispersion-induced optical phase decorrelation in a 60 GHz OFDM-RoF system. IEEE Photon. Technol. Lett. **26**(20), 2016–2019 (2014)
9. Sarup, V., Gupta, A.: A study of various trends and enabling technologies in radio over fiber (RoF) systems. Optik **126**(20), 2606–2611 (2015)
10. Shao, T., Martin, E.P., Anandarajah, P.M., Barry, L.P.: 60-GHz direct modulation-direct detection OFDM-RoF system using gain-switched laser. IEEE Photon. Technol. Lett. **27**(2), 193–196 (2015)
11. Huang, H., Sun, C., Lin, C., Wei, C., Zeng, W., Chang, H., Shih, B., Ngoma, A.: Direct-detection PDM-OFDM RoF system for 60-GHz 2x2 MIMO wireless transmission without polarization tracking. J. Lightw. Technol. **36**(17), 3739–3745 (2018)
12. Ji, W., Li, X., Kang, Z., Xue, X.: Design of WDM-RoF-PON based on improved OFDM mechanism and optical coherent technology. IEEE/OSA J. Opt. Commun. Netw. **7**(2), 74–82 (2015)
13. Browning, C., Elwan, H.H., Martin, E.P., ODuill, S., Poette, J., Sheridan, P., Farhang, A., Cabon, B., Barry, L,P.: Gain-switched optical frequency combs for future mobile radio-over-fiber millimeter-wave systems. J. Lightw. Technol. **36**(19), 4602–4610 (2018)
14. Hangting, H., Fengguang, L., Liu, Y., Shuailong, Y., Bin, L.: RF-pilot-based partition phase correction for CO-OFDM system phase noise mitigation. Opt. Eng. **57**(5), 1–7 (2018)
15. Peng, W., Tsuritani, T., Morita, I.: Simple carrier recovery approach for RF-pilot-assisted PDM-CO-OFDM systems. J. Lightw. Technol. **31**(15), 2555–2564 (2013)
16. Fan, Q., He, J., Chen, M., Liu, J., Chen, L.: Low-complexity phase noise compensation approach for CO-OFDM systems. IEEE Photon. Technol. Lett. **28**(21), 2323–2326 (2016)
17. Le, S.T., Kanesan, T., Giacoumidis, E., Doran, N.J., Ellis, A.D.: Quasi-pilot aided phase noise estimation for coherent optical OFDM systems. IEEE Photon. Technol. Lett. **26**(5), 504–507 (2014)
18. Yi, X., Shieh, W., Tang, Y.: Phase estimation for coherent optical OFDM. IEEE Photon. Technol. Lett. **19**(12), 919–921 (2007)
19. Liu, Y., Yang, C., Li, H.: Cost-effective and spectrum-efficient coherent TDM-OFDM-PON aided by blind ICI suppression. IEEE Photon. Technol. Lett. **27**(8), 887–890 (2015)
20. Al-Moliki, Y.M., Alresheedi, M.T., Al-Harthi, Y.: Secret key generation protocol for optical OFDM systems in indoor VLC networks. IEEE Photon. J. **9**(2), 1–15 (2017)
21. Islam, S.M.R., Kwak, K.S.: Two-stage channel estimation with estimated windowing for MB-OFDM UWB system. IEEE Commun. Lett. **20**(2), 272–275 (2016)
22. Liu, J., Mei, K., Zhang, X., Ma, D., Wei, J.: Online extreme learning machine-based channel estimation and equalization for OFDM systems. IEEE Commun. Lett. **23**(7), 1276–1279 (2019)
23. Zabala-Blanco, D., Mora, M., Azurdia-Meza, C.A., Dehghan Firoozabadi, A.: Extreme learning machines to combat phase noise in RoF-OFDM schemes. Electronics **8**, 9 (2019)
24. Zabala-Blanco, D., Campuzano, G., Aldaya, I., Castanon, G., Vargas-Rosales, C.: Impact of partial phase decorrelation on the performance of pilot-assisted millimeter-wave RoF-OFDM systems. Phys. Commun. **26**, 106–115 (2018)
25. Omomukuyo, O., Thakur, M.P., Mitchell, J.E.: Simple 60-GHz MB-OFDM ultrawideband RoF system based on remote heterodyning. IEEE Photon. Technol. Lett. **25**(3), 268–271 (2013)
26. Mikroulis, S., Omomukuyo, O., Thakur, M.P., Mitchell, J.E.: Investigation of a SMF-MMF link for a remote heterodyne 60-GHz OFDM RoF based Gigabit wireless access topology. J. Lightw. Technol. **32**(20), 3645–3653 (2014)
27. Teng, Y., Chen, Y., Zhang, B., Li, J., Lu, L., Zhang, P.: Tunable single-mode injection-locked optoelectronic oscillator with low phase-noise. Optik **127**(10), 4312–4314 (2016)
28. Gallion, P., Mendieta, F.J., Leconte, R.: Single-frequency laser phase-noise limitation in single-mode optical-fiber coherent-detection systems with correlated fields. J. Opt. Soc. Am. **72**(9), 1167–1170 (1982)
29. Beas, J., Castanon, G., Aldaya, I., Aragon-Zavala, A., Campuzano, G.: Millimeter-wave frequency radio over fiber systems: a survey. IEEE Commun. Surv. Tutor. **15**(4), 1593–1619 (2013)
30. Thomas, V.A., El-Hajjar, M., Hanzo, L.: Millimeter-wave radio over fiber optical upconversion techniques relying on link nonlinearity. IEEE Commun. Surv. Tutor. **18**(1), 29–53 (2016)
31. Tzimpragos, G., Kachris, C., Djordjevic, I.B., Cvijetic, M., Soudris, D., Tomkos, I.: A survey on FEC codes for 100 G and beyond optical networks. IEEE Commun. Surv. Tutor. **18**(1), 209–221 (2016)
32. Shafik, R.A., Rahman, M.S., Islam, A.R.: On the extended relationships among EVM, BER and SNR as performance metrics. In: International Conference on Electrical and Computer Engineering, pp. 408–411 (2006)
33. Shao, T., Paresys, F., Maury, G., Guennec, Y.L., Cabon, B.: Investigation on the phase noise and EVM of digitally modulated millimeter wave signal in WDM optical heterodyning system. J. Lightw. Technol. **30**(6), 876–885 (2012)
34. Stark, H., Woods, J.: Probability, Statistics, and Random Processes for Engineers, 4th edn. Pearson Education, New Jersey (2012)
35. Antoniades, N., Ellinas, G., Roudas, I. (eds.): WDM Systems and Networks: Modeling, Simulation, Design and Engineering. Springer, New York (2012)

36. Banerjee, D.: PLL Performance, Simulation, and Design, 5th edn. Dog Ear Publishing, Indianapolis (2017)
37. Pollet, T., Van Bladel, M., Moeneclaey, M.: BER sensitivity of OFDM systems to carrier frequency offset and Wiener phase noise. IEEE Trans. Commun. **43**(2/3/4), 191–193 (1995)
38. Al-Hosiny, N.M.: Effect of linewidth enhancement factor on the stability map of optically injected distributed feedback laser. Opt. Rev. **21**(3), 261–264 (2014)
39. Park, S.H., Jeon, H.: Microchip-type InGaN vertical external-cavity surface-emitting laser. Opt. Rev. **13**(1), 20–23 (2006)
40. Peng, W.: Analysis of laser phase noise effect in direct-detection optical OFDM transmission. J. Lightw. Technol. **28**(17), 2526–2536 (2010)
41. Kamal, S., Azurdia-Meza, C., Lee, K.: Improved Nyquist-I pulses to enhance the performance of OFDM-based systems. Wirel. Pers. Commun. **95**(4), 4095–4111 (2017)